Quaternary Research 75 (2011) 288–300

Contents lists available at ScienceDirect

Quaternary Research

journal homepage: www.elsevier.com/locate/yqres

A multi-proxy approach to assessing isolation basin stratigraphy from the Lofoten Islands, Norway

Nicholas L. Balascio [a,*], Zhaohui Zhang [a,1], Raymond S. Bradley [a], Bianca Perren [b], Svein Olaf Dahl [c,d], Jostein Bakke [c,d]

[a] Climate System Research Center, Department of Geosciences, University of Massachusetts, Amherst, MA, 01003, USA
[b] Laboratoire Chrono-Environnement, Université de Franche-Comté, 25030 Besançon, France
[c] Bjerknes Centre for Climate Research, N-5007 Bergen, Norway
[d] Department of Geography, University of Bergen, N-5007 Bergen, Norway

ARTICLE INFO

Article history:
Received 14 November 2009
Available online 24 September 2010

Keywords:
Relative sea level
Isolation basin
Holocene
Lofoten Islands
Norway

ABSTRACT

This study takes a comprehensive approach to characterizing the isolation sequence of Heimerdalsvatnet, a coastal lake in the Lofoten Islands, northern Norway. We use established methods and explore new techniques to assess changes in marine influence. Bathymetric and sub-bottom profiles were acquired to examine basin-wide sedimentation and a 5.8 m sediment core spanning the last 7800 cal yr BP was analyzed. We measured magnetic susceptibility, bulk organic matter properties, molecular biomarkers, diatom assemblages, and elemental profiles acquired by scanning X-ray fluorescence. These characteristics of the sediment reflect detailed changes in salinity and water column conditions as the lake was progressively isolated. Three distinct litho/chemo-stratigraphic units represent a restricted marine phase (7800–6500 cal yr BP), a transitional phase characterized by intermittent marine influence (6500–4900 cal yr BP), and complete isolation and freshwater sedimentation (4900 cal yr BP to present). Although there are uncertainties in the estimate of the threshold elevation of the lake, the timing of these phases generally corresponds with previous interpretations of the local relative sea-level history. This record captures sea-level regression following the Tapes transgression and supports the interpretation of a subsequent sea-level stillstand, dated in Heimerdalsvatnet from 6500 to 4900 cal yr BP.

Introduction

Relative sea-level histories can be reconstructed from a variety of coastal sedimentary environments: raised beaches, wave cut terraces, estuaries and isolation basins. Isolation basins are particularly useful because they provide continuous sedimentary archives of marine–lacustrine transitions, the transgression and isolation contacts can usually be well-dated, and basin thresholds provide information on former sea-level elevations. In addition, isolation basin records are analogues for processes affecting coastal environments that are being impacted by present rising or falling sea level.

Reconstructing the environmental history of isolation basins requires the identification of changes in marine influence (i.e. marine, brackish, and freshwater facies), which can be difficult since sea-level fluctuations affect water column chemistry, organic matter input, and sediment source. Methods of characterizing isolation basin stratigraphy traditionally rely on microfossil assemblages and their relationship to salinity (e.g. Kjemperud, 1981; Svendsen and Mangerud, 1990; Shennan et al., 1995; Corner et al., 1999, 2001; Long et al., 1999; Zong and Horton, 1999; Lloyd, 2000; Hutchinson et al., 2004). However, counting and identifying microfossils is time consuming and can be affected by microfossil abundance, preservation, non-analogue situations, and when species have wide salinity tolerances.

Recently, different approaches have emerged to overcome limitations of microfossil records and to better characterize paleoenvironmental conditions. Properties of bulk sedimentary organic matter, mainly $\delta^{13}C$ and C/N ratios, have been used to identify salinity changes and in most cases correlate well to microfossil reconstructions (Westman and Hedenström, 2002; Mackie et al., 2005, 2007; Wilson et al., 2005; Lamb et al., 2006 and references therein; Mills et al., 2009). This method is more rapid, but also has limitations such as selective degradation of organic matter and can be affected by large external environmental changes including atmospheric pCO_2, vegetation development, and temperature (Lamb et al., 2006; Mackie et al., 2007). Others have also explored the use of molecular biomarkers (Bendle et al., 2009) as indicators of surface water salinity and scanning X-ray fluorescence (XRF) (Sparrenbom et al., 2006) to identity physical sedimentary changes.

* Corresponding author.
E-mail address: balascio@geo.umass.edu (N.L. Balascio).
[1] Current address: Department of Earth Sciences, Nanjing University, Nanjing, 210093, China.

0033-5894/$ – see front matter © 2010 University of Washington. Published by Elsevier Inc. All rights reserved.
doi:10.1016/j.yqres.2010.08.012

This study applies a range of methods for reconstructing environmental conditions in an isolation sequence. We present results from Heimerdalsvatnet, a coastal lake located in the Lofoten Islands, northern Norway. This area is near the former margin of the Scandinavian Ice Sheet and has experienced a complex relative sea-level history, which has even been linked to prehistoric and Viking-age settlements (Utne, 1973; Møller, 1987; Mills et al., 2009). We use bathymetric and sub-bottom profiles to characterize basin-wide sedimentation and analyzed a 5.8 m sediment core using multiple techniques, including: bulk sediment organic geochemistry, diatoms, molecular biomarkers, and high-resolution XRF core scans. This comprehensive approach enables us to characterize environmental conditions and water column properties during isolation, compare the effectiveness of each method for interpreting isolation basin stratigraphy, and contribute to the local sea-level history.

Setting

The Lofoten–Vesterålen archipelago (67–70°N) extends from northeast to southwest into the Norwegian Sea (Fig. 1A). The Lofoten Islands are separated from the mainland by Vestfjord and consist of seven islands; the second largest is Vestvågøya (Fig. 1B). Postglacial marine limits in Lofoten and Vesterålen generally increase from 10 m a.s.l. in the northwest to 45 m a.s.l. in the southeastern areas (Møller, 1986) following a trend similar to the pattern of present uplift rates occurring in northern Norway (Vestøl, 2006). The most recent sea-level investigations (Møller, 1984, 1985, 1986, 1987, 1989; Vorren and Moe, 1986; Vorren et al., 1988) built upon and revised earlier work (Marthinussen, 1962; Bergström, 1973; Utne, 1973). In Vestvågøya, and areas along a similar isobase, these sea-level reconstructions show a relative regression from ~37 m a.s.l. after deglaciation to ~ −3 m a.s.l. in the early Holocene. This was followed by the Tapes transgression that reached its maximum at ~6800 cal yr BP (~6000 ^{14}C years BP) after which relative sea level decreased during the mid- and late Holocene. The Tapes shoreline isobases in northern Norway increase from 0 m in the northwest to 20 m in the southeast (Møller, 1987) (Fig. 1B). The local Holocene shoreline displacement curve is developed from dated lithostratigraphic sequences from Vestvågøya, Andøya, and Flagstadøya and shows the Tapes maximum reached 9–10 m above mean tide level (Møller, 1986).

Heimerdalsvatnet

Heimerdalsvatnet (68°17.78′N, 13°39.38′E; 5 m a.s.l.) is located on the northern coast of Vestvågøya 1.5 km from the town of Eggum (Fig. 1C) and is impounded by a beach ridge with a crest elevation of 8 m a.s.l. There are numerous raised shoreline features along this section of coast, the most prominent of which is the relict dune field that underlies Eggum. This feature is mapped at 10 m above m.t.l. (Møller, 1985) and a peat deposit found beneath a prominent beach ridge in Eggum has been dated to 6800 cal yr BP (Bergström, 1973), corresponding to the local Tapes transgression maximum (Møller, 1986). Heimerdalsvatnet is 1.5 km long, 0.5 km wide, and the deepest part of the lake is 36.7 m. There is a small inlet to the lake on the southeastern edge that is presently fed by two smaller artificially dammed lakes in the upper valley. Lateral moraines on both sides of the lake near the mouth of the valley have been modified during a period of higher sea level. These glacial deposits are associated with the youngest moraines found in Lofoten and have been most recently mapped as late glacial or Younger Dryas in age (Bargel, 2003).

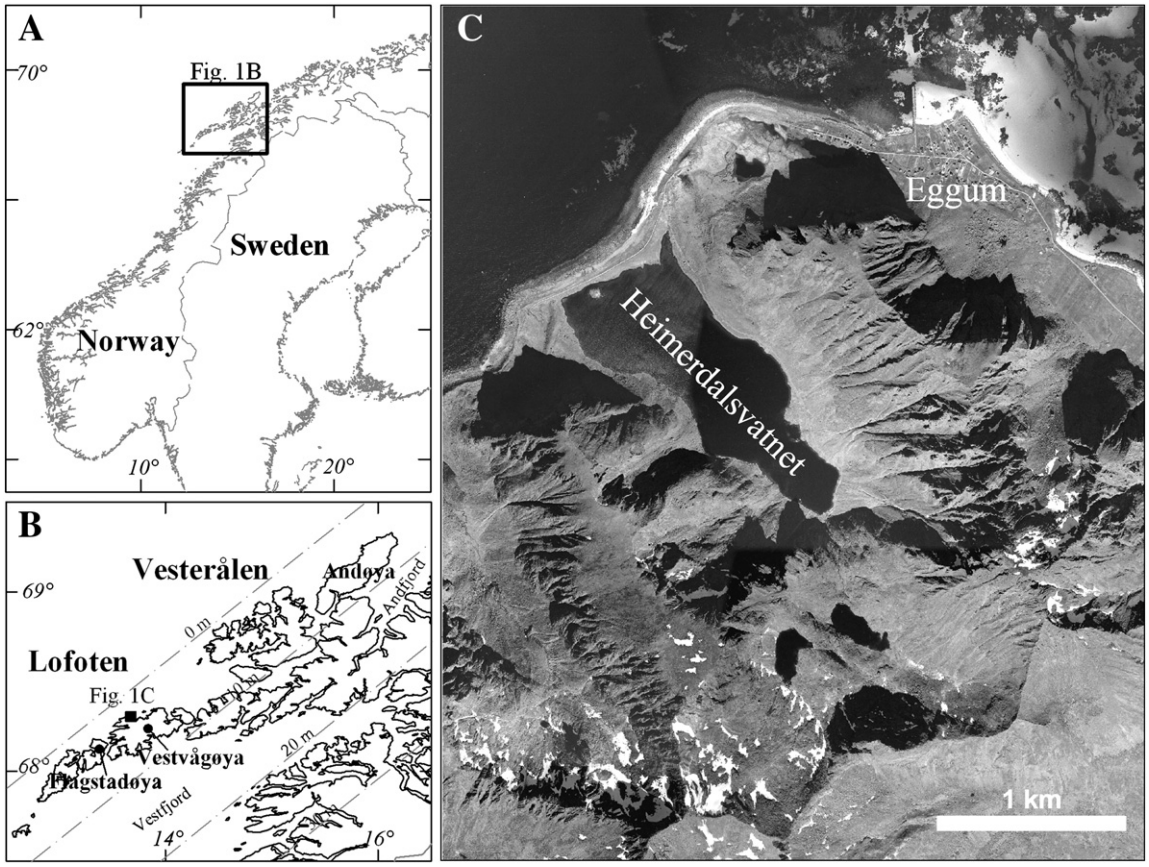

Figure 1. (A) The Lofoten–Vesterålen archipelago off the northwestern coast of Norway. (B) Vestvågøya in the Lofoten Islands. Dashed lines are isobases of the Tapes transgression maximum reconstructed from sites across northern Norway and represent the general regional trend of this shoreline (from Møller, 1987). (C) Air photograph of Heimerdalsvatnet showing the location of the town of Eggum.

The present water column conditions of Heimerdalsvatnet were assessed in August 2007 (Fig. 2). Water column profiles measured at the deepest location show a thermocline at ~14 m water depth. The pH ranges from 5.6 to 6.3 and conductivity from 52 to 57 µs/cm. Dissolved oxygen ranges from 11.7 to 13.7 mg/L with an average value of 12.1 mg/L in the epilimnion. Data-logging thermistors were deployed throughout the water column and recorded temperatures from September 2007 through 2008. Nine thermisters spaced throughout the water column were suspended from a buoy anchored at the deepest location and recorded temperature every 4 hours. Monthly average temperature contours show the annual temperature fluctuations, which are typical for a dimictic lake.

Methods

Basin analysis and sediment coring

Bathymetry was recorded using a fish-finder acoustic sounder with integrated GPS. Sub-bottom profiles were obtained using an Edgetech 3100 seismic system with towfish model SB-424 (4–24 kHz). Travel time was converted to sediment depth using 1650 ms^{-1} for the speed of sound in sediment. In 2007, a 5.8 m sediment core (NHP-207) was recovered using a modified Nesje percussion coring device. The core was sectioned, split, described, photographed, and the magnetic susceptibility of the split cores was measured every 0.5 cm using a Bartington MS2E sensor.

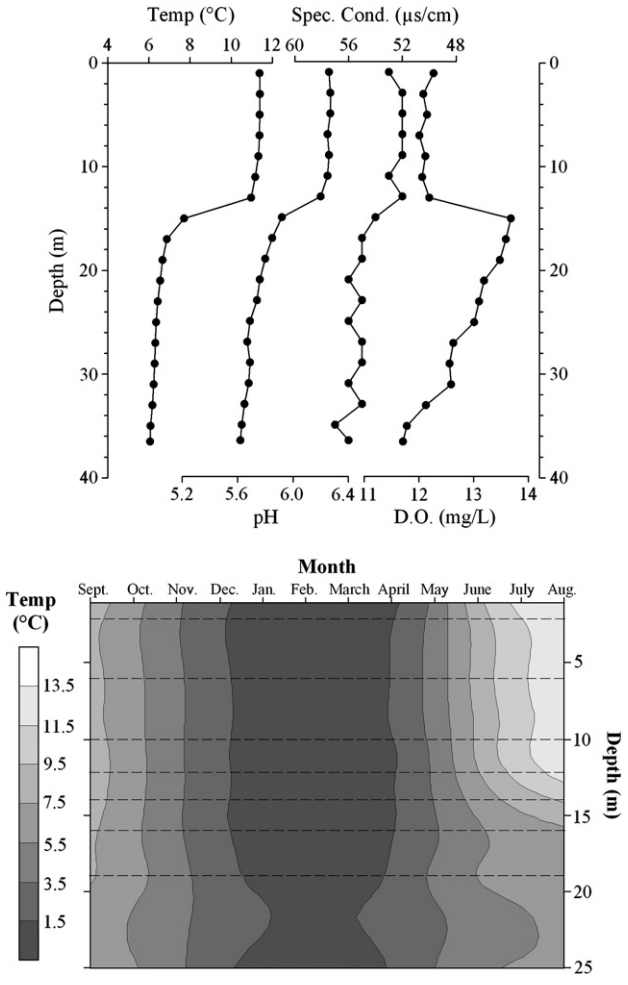

Figure 2. (Top) Water column profiles from Heimerdalsvatnet taken in August 2007. (Bottom) Monthly average lake water temperature contours from Heimerdalsvatnet recorded from September 2007 through August 2008. Dashed lines show thermister depths.

Chronology

Five radiocarbon samples were analyzed and ages were calibrated to calendar years using CALIB v. 5.0.2 (Stuiver and Reimer, 1993) with the IntCal04 calibration dataset (Reimer et al., 2004). A marine reservoir correction was applied to one date on a marine shell. We searched for tephra to support the radiocarbon chronology and targeted two depth intervals between radiocarbon samples (16–45 cm; 140–153 cm). Previous studies from this area (Pilcher et al., 2005; Mills et al., 2009) have shown that tephra are only present in low concentrations as cryptotephra (Alloway et al., 2006) so that isolation from organic and minerogenic components of the sediment is necessary. Contiguous 1 cm samples were acidified (Pilcher et al., 1996), washed in deionized water over a 20 µm sieve, and subjected to heavy liquid separations using sodium polytungstate between 2.3 and 2.5 g/cm^3 to concentrate tephra grains (Turney, 1998). Samples were mounted on slides and tephra were counted using a light microscope. Select slides containing tephra were analyzed with a Cameca SX50 electron microprobe and their major oxide concentrations were compared to samples of known age found around the North Atlantic region.

Diatoms

Six samples were chosen for diatom analysis from 70, 140, 230, 240, 310, and 400 cm depth in the core. Diatoms were isolated from the sediments using standard oxidative techniques (Renberg, 1990), whereby samples were treated with 30% H_2O_2, heated until the reaction subsided, then treated with HCl to remove carbonates. Samples were repeatedly rinsed with water, aliquots were dried on glass coverslips, and mounted with Naphrax mounting medium. At least 400 diatom valves were identified from each slide using marine and freshwater reference floras.

Bulk organic geochemistry

The core was sub-sampled every 25 cm for bulk organic geochemical analysis. Samples were dried in a low temperature oven, ground, and an aliquot was measured on a Costech ECS 4010 Elemental Analyzer for total carbon (%TC) and total nitrogen (%TN). Another aliquot of samples were acidified with concentrated sulfurous acid to remove carbonate and measured for total organic carbon (%OC). Standard deviations based on triplicate analysis of %C, %TN, and %OC measurements were ±0.2%. Total inorganic carbon (%IC) was calculated as the difference between % C and %OC. $\delta^{13}C_{org}$ and $\delta^{15}N_{org}$ were measured on acidified and unacidified samples, respectively, using a Thermo Delta V Advantage IRMS interfaced with the element analyzer, and reported relative to VPDB for $\delta^{13}C_{org}$, and AIR for $\delta^{15}N_{org}$. Standard deviations based on triplicate analysis were less than 0.03‰ for $\delta^{13}C_{org}$ and 0.05‰ for $\delta^{15}N_{org}$.

Molecular biomarkers

Molecular biomarker analyses were performed on 31 samples. Lipid extraction and analyses followed the protocol described in Zhang and Sachs (2007). Freeze-dried lake sediments were extracted on a Dionex ASE-200 pressurized fluid extractor with dichloromethane (DCM) and methanol (MeOH) (9:1) at 1200 psi and 100°C. The total lipid extract was fractionated on an aminopropyl cartridge-style SPE column (Burdick and Jackson, size 500 mg/4 ml) with DCM/isopropyl alcohol (IPA) (3:1). The DCM/IPA fraction was fractionated by silica gel column chromatography. Hydrocarbons were eluted with hexane. Each fraction was analyzed by an Agilent 6890 gas chromatography–mass spectrometry (GC–MS) for biomarker identification, then by an Agilent GC with flame-ionization detection (GC-FID) to determine concentrations.

Scanning X-ray fluorescence

Relative elemental composition of the sediment was determined by X-ray fluorescence (XRF) using an Itrax™ core scanner at the Institut National de la Recherche Scientifique, Quebec City, Canada. This technique uses an intense micro-X-ray beam to scan a sediment core surface to generate elemental profiles at sub-millimeter resolution (Croudace et al., 2006). At each measurement point, a dispersive energy spectrum is generated and peak area integrals are calculated for each element reflecting their relative concentration in the sediment. These results are considered semi-quantitative because they are also influenced by characteristics of the sediment matrix such as particle size, water content, mineralogy, and density. Although, no significant X-ray count rate changes were observed during scanning of the core that would influence the interpretation of the elemental results. Eight overlapping U-channels that span the length of core NHP-207 were analyzed every 0.5 mm on the Itrax using an exposure time of 20 s, voltage of 35 kV, and current of 45 mA. We focused our analysis on elements: Al, Si, S, Cl, K, Ca, Ti, Mn, Fe, Ni, Zn, Br, Rb, and Sr.

Results and discussion

Analysis of seismic profiles, diatoms, bulk organic geochemistry, molecular biomarkers, and scanning XRF profiles show that core NHP-207 contains three distinct phases of sedimentation: Unit I (576–373 cm), Unit II (373–186 cm), and Unit III (186–0 cm) with Unit II having two sub-units: Unit II_a (373–310 cm) and Unit II_b (310–186 cm). Here we describe how each proxy records changes across these units and their relevance for understanding past environmental conditions.

Basin analysis

The southeast end of the lake has three main basins that are 26.1 m, 30.1 m, and 36.7 m deep (Fig. 3). Northwest of these basins the depth decreases towards the beach ridge that impounds the lake. Core NHP-207 was collected from the northernmost basin. Sub-bottom profiles across the two deepest basins show sediment thicknesses of ~5.8 m and ~8.7 m, respectively, and both profiles have three acoustically distinct units (Fig. 3). The lower unit appears massive with some faint layering. This unit abruptly transitions into the middle unit that has strong sub-horizontal acoustic reflections. The upper unit is more massive with some weaker discontinuous acoustic reflections. The seismic transect near our coring location indicates that the lower, middle, and upper units are ~2.9 m, 1.5 m, and 1.5 m thick, respectively.

Chronology

AMS dates indicate that the record spans the last ~7800 cal yr BP (Table 1). An age–depth model was developed based on linear interpolation between radiocarbon dates (Fig. 4). Three tephra horizons support the radiocarbon age model (Table 2; Fig. 4). Significant quantities of tephra were found in samples 35–36, 37–38, 39–40, 141–142, and 148–149 cm. Samples from 35–36, 37–38, and 39–40 cm contain pinkish brown vesicular tephra that have distinct TiO_2 and MgO values. These tephra are similar in composition to the GA4–85 tephra found in Ireland with an age range of A.D. 700–800 (Hall and Pilcher, 2002). A second geochemical population occurs at 39–40 cm where the geochemistry is similar to the BIP-24a tephra previously found in peat bog and lake sediments from Lofoten (Pilcher et al., 2005). The age of this tephra is estimated to be around A.D. 900. Lower in the core, pinkish brown vesicular tephra were found and a peak in concentration occurred in the sample from 148–149 cm. The compositions of grains in samples from 141–142 and 148–149 cm match tephra from the Katla volcanic system and probably correspond to the SILK-N2 tephra (Larsen et al., 2001). Tephra from this eruption has been dated in Iceland to ~4200 cal yr BP and has also been found at a site in Ireland (Plunkett et al., 2004). Direct application of these tephra horizons to the chronology of core NHP-207 is difficult because of dating uncertainty and the additional stratigraphic uncertainty due to their vertical distribution within the sediment from landscape reworking and/or downward migration of particles in the sediment (Davies et al., 2007). However, these age estimates confirm the trends in our radiocarbon-based chronology.

Diatoms

Diatoms are reliable indicators of salinity conditions and the select samples from core NHP-207 provide an initial understanding of salinity changes across the record (Fig. 5). Diatom assemblages analyzed at 400 cm are characterized by a mix of both planktonic and benthic marine taxa (*Chaetoceros* spp. resting spores, *Thalassiosira* spp., marine *Cocconeis* spp.). The sample from 310 cm contains diatoms that represent a true freshwater flora (*Cyclotella pseudostelligera*, *Fragilaria virescens* var. *exigua*, *Achnanthes* spp.). Diatoms from 230 and 240 cm have both brackish (*Diatoma elongatum)* and freshwater (*Fragilaria virescens* var. *exigua* and *Cyclotella pseudostelligera*) affinities. The upper two diatom samples, 70 and 140 cm, contain both benthic and

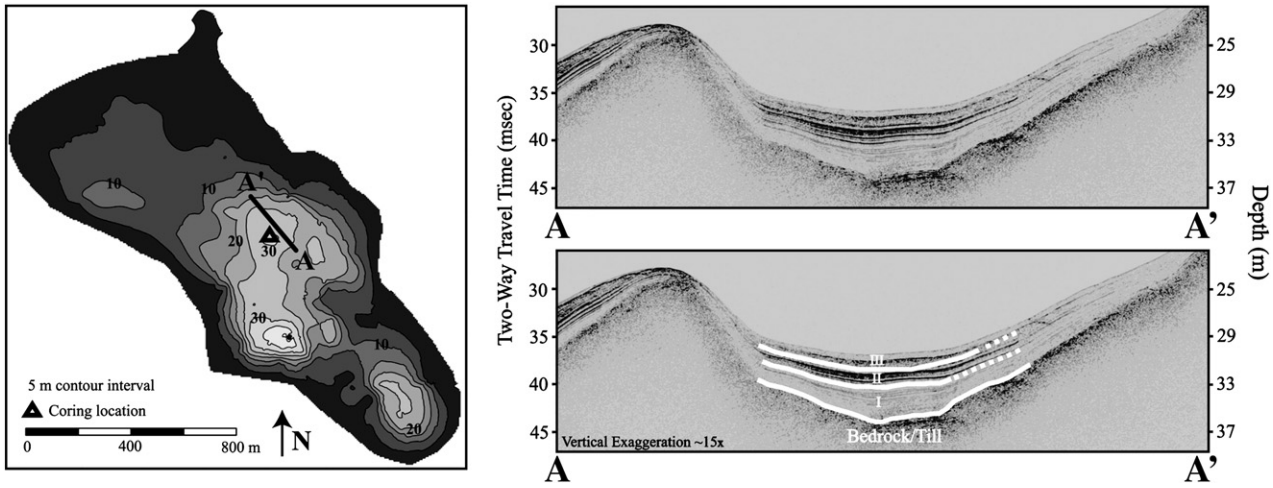

Figure 3. (Left) Bathymetric map of Heimerdalsvatnet showing the location of sediment core NHP-207and a sub-bottom profile (A to A′). (Right) Sub-bottom profile near the coring location and our interpretation of three stratigraphic units, I–III.

Table 1
Radiocarbon results for core NHP-207 (calibrated with CALIB 5.0.2).

Depth (cm)	Description	Laboratory #	$\delta^{13}C$ ‰	^{14}C yr BP	Cal Age Range (1 σ)	Cal Age Range (2 σ)	Median 1-σ Age (cal yr BP)
73.5	Plant/Wood	OS-67689	−26.52	1760 ± 30	1619–1713	1567–1806	1666 ± 47
130	Plant/Wood	OS-67681	−24.39	3610 ± 35	3874–3972	3834–4068	3923 ± 49
205	Plant/Wood	Beta-241113	NA	4550 ± 40	5067–5314	5049–5434	5191 ± 124
292	Plant/Wood	OS-67690	−24.46	5260 ± 35	5941–6174	5931–6178	6058 ± 117
570	Shell[a]	Beta-241115	−1.5	7350 ± 50	7673–7818	7616–7902	7746 ± 73

[a] Marine reservoir correction applied (Delta-R = 65 ± 44).

planktonic freshwater species, dominated by *Fragilaria virescens* var. *exigua*, small *Achnanthes* spp., and *Cyclotella cyclopuncta*. There are also smaller numbers of both *Frustulia* sp. and *Aulacoseira* spp.

The diatom taxa generally show a decreasing marine influence across the three stratigraphic units (Fig. 5). They transition from marine, to brackish, and then freshwater species in Units I, II_b, and III, respectively. The one anomaly is the sample analyzed from 310 cm, which shows the appearance of freshwater assemblages between samples that have species indicative of marine (Unit I) and brackish conditions (Unit II_b).

Sedimentary and bulk organic geochemical stratigraphy

The sediment in core NHP-207 is brown and organic-rich throughout, and does not have visibly distinct stratigraphic boundaries. However, there are minor changes in lithology and significant changes in magnetic susceptibility and organic geochemistry across Units I–III. (Fig. 4). Sediment in Unit I is light brown, dense, with isolated shells and shell fragments and has low magnetic susceptibility. %OC values average 6.0% and increase from the base of the core. %IC values are variable and only a small percentage of the total carbon content of the sediment, but are highest in this unit. C/N values average 9.6. Both $\delta^{13}C_{org}$ and $\delta^{15}N_{org}$ are highest in Unit I with average values of −22.86‰ and 6.55‰, respectively. Unit II is a transitional zone. In Unit II_a, there is a weak cm-scale banding of alternating light and dark brown horizons. This interval is associated with a rise in magnetic susceptibility. In Unit II_b, the sediment is darker brown and has extremely low magnetic susceptibility. The top of Unit II_b is marked by a 0.5-cm-thick dark brown organic-rich layer capped by a coarse 1-mm-thick sandy lamination. Bulk organic geochemical properties within Unit II are marked by an abrupt decrease in $\delta^{13}C_{org}$ and $\delta^{15}N_{org}$ by 2.29‰ and 3.26‰, respectively. %OC values are higher than in Unit I and C/N values slightly increase within Unit II_b. Unit III is characterized by higher, more variable magnetic susceptibility values that correspond to layers with coarser sediment and terrestrial macrofossils. There is also a decrease in average $\delta^{13}C_{org}$ and $\delta^{15}N_{org}$ values.

Organic geochemical data, mainly $\delta^{13}C_{org}$, support the interpretation of decreasing marine influence between Units I–III. $\delta^{13}C_{org}$ values primarily represent an algae signal since C/N ratios across the record are ~10, which are typical for algae whereas organic matter sourced from terrestrial plants has values greater than 20 (Meyers, 1994). There is a rise in the C/N ratios in Unit II_b that may indicate a slight increase in the proportion of terrestrial material delivered to the basin, but even during this interval values do not exceed 14. Algae have $\delta^{13}C_{org}$ values that are ~20‰ less than their dissolved inorganic carbon source, which is dissolved CO_2 (−7‰) in freshwater environments and bicarbonate (1‰) in marine environments. Therefore marine algae generally have higher $\delta^{13}C_{org}$ values (−22‰ to −20‰) than freshwater algae (−30‰ to −25‰) (Meyers 1994). Mackie et al. (2005) correlated $\delta^{13}C_{org}$ to salinity, as reconstructed using diatom flora from an isolation basin in Scotland, and further categorized marine (−22‰ to −16‰), brackish (−25‰ to −22‰), and freshwater (−30‰ to −25‰) $\delta^{13}C$ zones.

In Heimerdalsvatnet, $\delta^{13}C_{org}$ values in Unit I resemble those typical of algae in marine or brackish conditions. The decrease in values across Units II and III show the change to less saline conditions. These trends are also reflected in $\delta^{15}N_{org}$ values. $\delta^{15}N_{org}$ is a less commonly applied proxy due to complexities in nitrogen cycling (Talbot, 2001; Meyers, 2003), but has been used in isolation basin studies (Westman

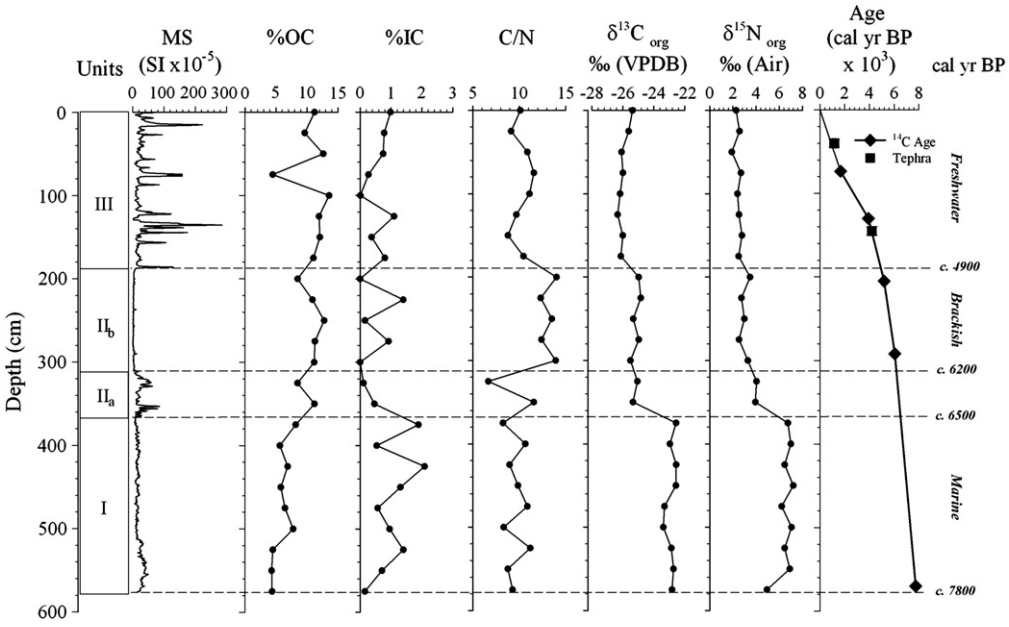

Figure 4. Magnetic susceptibility, bulk organic geochemical results, and age–depth model plotted with the defined stratigraphic units I–III. The age–depth relationship is based on linear interpolation between radiocarbon dates from core NHP-207. Error bars show 1σ age range. Two tephra horizons identified in core NHP-207 are displayed to support the chronology.

Table 2
Electron microprobe results for tephra analyzed from core NHP-207. The tephra results fall into three compositional populations and the average and standard deviation are presented for each population.

Sample	P_2O_5	SiO_2	TiO_2	Al_2O_3	MgO	CaO	MnO	FeO	Na_2O	K_2O	Cl	Total
36 cm	0.35	65.27	1.12	14.22	1.21	3.44	0.16	6.01	3.31	2.61	0.08	97.78
38 cm	0.26	65.54	1.12	14.16	1.23	3.51	0.21	5.96	3.54	2.55	0.09	98.18
	0.30	65.58	1.20	14.39	1.20	3.35	0.22	5.62	3.99	2.70	0.07	98.62
	0.27	66.03	1.11	14.42	1.12	3.23	0.23	5.46	3.89	2.72	0.06	98.53
	0.29	64.54	1.10	13.97	1.10	3.20	0.23	5.51	4.21	2.64	0.06	96.84
	0.24	66.32	1.17	14.26	1.19	3.31	0.19	5.58	4.00	2.65	0.07	98.97
	0.25	66.40	1.25	14.56	1.16	3.34	0.23	5.67	3.68	2.64	0.07	99.25
40 cm	0.32	66.33	1.14	14.27	1.10	3.21	0.19	5.45	2.70	2.70	0.07	97.50
Group 1	0.29	66.10	1.20	14.14	1.11	3.21	0.15	5.54	2.87	2.73	0.10	97.44
	0.28	66.88	1.13	14.35	1.04	2.96	0.20	5.19	2.46	2.76	0.09	97.33
	0.39	65.52	1.13	14.16	1.15	3.31	0.16	5.40	2.99	2.72	0.07	97.01
	0.30	66.11	1.21	14.45	1.14	3.30	0.15	5.54	3.47	2.79	0.12	98.57
	0.32	66.12	1.20	14.27	1.16	3.27	0.15	5.66	3.19	2.66	0.10	98.10
Average	*0.30*	*65.90*	*1.16*	*14.28*	*1.15*	*3.28*	*0.19*	*5.58*	*3.41*	*2.68*	*0.08*	*98.01*
(1 σ)	*0.04*	*0.60*	*0.05*	*0.16*	*0.05*	*0.13*	*0.03*	*0.22*	*0.55*	*0.07*	*0.02*	*0.76*
40 cm	0.12	67.40	0.40	16.09	0.26	1.98	0.15	4.28	2.87	3.95	0.22	97.73
Group 2	0.10	67.49	0.41	16.06	0.33	2.05	0.17	4.42	2.89	3.92	0.22	98.06
	0.09	64.46	0.43	15.37	0.35	2.04	0.14	4.37	2.72	3.83	0.29	94.09
	0.10	68.40	0.39	15.98	0.25	1.89	0.13	4.13	3.18	4.05	0.25	98.75
	0.09	66.23	0.39	15.58	0.26	1.84	0.16	4.13	2.65	3.77	0.26	95.36
	0.13	66.34	0.42	15.73	0.29	1.97	0.14	4.29	2.56	3.91	0.24	96.00
	0.08	67.13	0.39	16.00	0.25	1.85	0.14	4.23	2.44	4.06	0.22	96.79
	0.11	66.42	0.40	15.90	0.26	1.90	0.15	4.29	3.24	3.86	0.23	96.76
	0.08	66.83	0.38	15.81	0.25	1.87	0.16	4.13	2.53	3.98	0.26	96.29
	0.12	67.15	0.41	15.90	0.25	1.94	0.19	4.20	2.69	4.04	0.22	97.10
	0.11	72.64	0.28	12.99	0.39	2.28	0.09	1.99	2.05	2.00	0.29	95.10
	0.13	66.01	0.47	16.11	0.39	2.29	0.19	4.79	2.94	3.89	0.20	97.40
	0.12	67.25	0.30	14.83	0.26	3.08	0.12	4.86	2.61	2.09	0.06	95.59
	0.07	67.19	0.40	15.80	0.28	1.97	0.18	4.18	3.60	4.02	0.24	97.92
	0.11	67.00	0.39	16.06	0.31	2.05	0.16	4.60	3.32	4.03	0.23	98.24
Average	*0.10*	*67.20*	*0.39*	*15.61*	*0.29*	*2.07*	*0.15*	*4.19*	*2.82*	*3.69*	*0.23*	*96.75*
(1 σ)	*0.02*	*1.74*	*0.05*	*0.80*	*0.05*	*0.31*	*0.03*	*0.65*	*0.39*	*0.67*	*0.05*	*1.33*
142 cm	0.26	66.35	1.24	14.39	1.16	3.36	0.11	5.58	4.05	2.61	0.06	99.18
	0.25	65.71	1.19	14.40	1.12	3.15	0.15	5.29	4.21	2.74	0.05	98.27
	0.30	64.87	1.11	14.11	1.09	3.13	0.12	5.33	4.05	2.62	0.04	96.76
	0.31	65.18	1.14	14.21	1.15	3.29	0.12	5.62	4.21	2.77	0.06	98.05
	0.31	66.95	1.19	14.40	1.12	3.24	0.13	5.31	4.04	2.69	0.06	99.43
	0.28	67.27	1.16	14.31	1.14	3.07	0.15	5.46	4.21	2.76	0.07	99.87
	0.30	66.51	1.14	14.50	1.18	3.40	0.08	5.54	4.17	2.72	0.06	99.58
	0.29	65.99	1.17	14.19	1.18	3.24	0.13	5.56	4.14	2.64	0.07	98.60
	0.36	65.73	1.10	14.35	1.19	3.24	0.10	5.70	4.13	2.62	0.05	98.57
	0.25	65.71	1.16	14.45	1.16	3.24	0.14	5.36	4.19	2.65	0.08	98.39
	0.28	67.15	1.09	14.27	0.95	2.86	0.12	4.62	4.03	2.79	0.06	98.21
	0.16	66.21	1.13	14.38	1.16	3.27	0.17	5.40	4.45	2.69	0.05	99.08
	0.30	67.00	1.22	14.38	1.16	3.13	0.09	5.59	3.59	2.60	0.07	99.12
	0.29	66.38	1.21	14.53	1.18	3.23	0.13	5.61	4.54	2.55	0.06	99.70
	0.33	65.28	1.19	14.35	1.19	3.34	0.14	5.80	4.39	2.61	0.06	98.69
	0.27	65.02	1.24	14.36	1.10	3.30	0.12	5.42	3.81	2.64	0.06	97.33
	0.33	66.23	1.12	14.07	0.98	2.80	0.11	4.81	4.14	3.05	0.05	97.68
	0.27	66.01	1.15	14.09	1.17	3.35	0.14	5.62	4.05	2.65	0.07	98.54
149 cm	0.32	65.92	1.16	14.45	1.20	3.40	0.12	5.82	3.67	2.59	0.06	98.72
	0.31	65.92	1.04	14.58	1.15	3.21	0.17	5.65	3.46	2.69	0.07	98.24
	0.33	66.31	1.13	14.54	1.18	3.31	0.18	5.62	2.80	2.64	0.07	98.12
	0.28	66.36	1.15	14.55	1.17	3.28	0.18	5.63	3.42	2.67	0.06	98.76
	0.31	66.39	1.05	14.49	1.07	3.10	0.18	5.26	3.23	2.71	0.05	97.84
Average	*0.29*	*66.11*	*1.15*	*14.36*	*1.14*	*3.21*	*0.13*	*5.46*	*3.96*	*2.68*	*0.06*	*98.55*
(1 σ)	*0.04*	*0.65*	*0.05*	*0.15*	*0.06*	*0.15*	*0.03*	*0.28*	*0.42*	*0.10*	*0.01*	*0.76*

and Hedenström, 2002). In Heimerdalsvatnet, the $\delta^{15}N_{org}$ trend likely represents a change in the source of dissolved inorganic nitrogen with decreasing surface water salinity.

Molecular biomarkers

Hydrocarbon biomarkers are characterized by two main components, short and long-chain *n*-alkanes, and highly branched isoprenoid hydrocarbons (HBI), which can be related to marine and freshwater environments (Fig. 6A). GC–MS analyses also showed the presence of elemental sulfur from 570 to 370 cm, indicating an anoxic environment during this interval.

Short and medium-chain *n*-alkanes (C_{19} to C_{27}) are from freshwater algal sources (Zhang et al., 2004), while long-chain *n*-alkanes are from higher plant leaf waxes. The distribution of *n*-alkanes range from C_{23} to C_{33}, with centers at C_{27} and C_{31}, indicating an overall mixed source. There are also significant changes in concentration of short/medium-chain *n*-alkanes in the downcore profile (Fig. 7). They are in low abundance in Unit I with an average of 7.8 μg/g, increase in Unit II_a to a maximum value of 729 μg/g, and then vary from 23 to

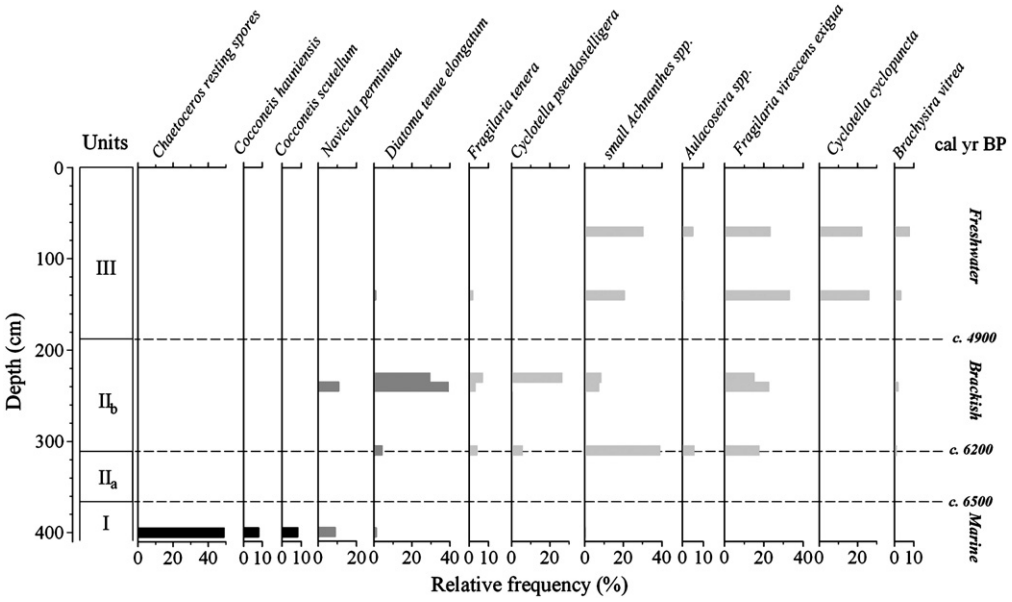

Figure 5. Percent abundance of diatom taxa that indicate different salinity conditions: marine (black), brackish (dark grey), and freshwater (light grey). Note the different percent abundance scales for each taxa.

107 μg/g with intermittent low values through Unit II$_b$. In Unit III, *n*-alkane concentrations decrease to intermediate concentrations with an average of 39.4 μg/g.

HBIs have been found in various marine and lacustrine hypersaline setting (Robson and Rowland, 1986; Xu et al., 2006). In core NHP-207, there are two types of HBIs, C_{25} and C_{20} (Figs. 6A and B). The $C_{25:1}$ HBIs likely originates from marine/brackish diatoms (Robson and Rowland, 1986; Xu et al., 2006). The C_{20} HBIs have been found in high abundance in coastal surface sediments (Gearing et al., 1976) and in Puget Sound (Barrick et al., 1980), but no clear algal producer has been identified. Although, both C_{20} and $C_{25:1}$ HBIs show similar downcore variations suggesting a common source from marine/brackish diatoms (Fig. 7). In Unit I, both HBIs are below detection limits. In Unit II$_a$, C_{20} and $C_{25:1}$ are detected in low concentrations (<1.1 μg/g) then rapidly increase within Unit II$_b$ to maxima of 63.8 and 37.4 μg/g, respectively, and then show an equally dramatic decrease in concentration. In Unit III, C_{20} HBIs are in very low abundance, while C_{25} HBIs show a slight increase at the base of Unit III and then quickly decrease to below detection limits from 140 cm to the top of the core.

Molecular biomarkers concentrations provide further evidence for decreasing marine influence, and show dramatic changes in surface water conditions during Unit II. The abrupt increase of *n*-alkanes and HBIs across Unit II indicates a period of unusually high productivity, probably due to changes in surface water salinity and/or nutrient supply. In Unit I, low quantities of *n*-alkanes support the interpretation that this was a dominantly marine interval. The lack of HBIs in Unit I and their rapid appearance in Unit II, which is a brackish interval based on other evidence, suggest that they are produced by species of brackish diatoms or that the organisms that produce them require high nutrient conditions. The decrease in concentration of HBIs in Unit III shows a change to freshwater conditions, which is also supported by the presence of *n*-alkanes during this interval.

Scanning XRF analysis

XRF data primarily reflect changes in the source and amount of detrital input, but a few marine-sourced elements also reflect changes in marine influence (Fig. 8). We present plots of the first principal component (PC1) scores, Ti, Ca, S, and Si/Ti profiles. These profiles were chosen based on statistical analysis of the XRF data (Tables 3 and 4) and to highlight elements that have trends similar to changes in organic geochemical data. We performed a principal component analysis (PCA) to statistically define the primary trend in the elemental data (Table 4). PCA of the entire dataset shows that the first eigenvector accounts for 77% of the total variance. This variance is mainly controlled by K, Ti, Mn, Fe, Ni, Zn, and Sr, which all have high factor loads (>0.900) and are highly correlated to one another (Tables 3 and 4). Trends in the elemental dataset are therefore strongly controlled by physical sedimentation and the similarity between PC 1 scores and Ti, a common indicator of detrital input, exemplify these changes (Fig. 8). Values for PC1 and Ti are highest at the base of Unit I. They gradually decrease and then sharply decline at the base of Unit II. Within Unit II values are relative low and less variable. Unit III is marked by high amplitude variations similar to magnetic susceptibility. The decline in Ti values across Unit I is likely affected by the increase in organic content of the sediment across this interval resulting from increased aquatic productivity as surface waters became less saline. Unit II is a period when sedimentation rates were still high, but probably dominated by organic sedimentation since Ti values are low. In Unit III, sedimentation has slowed and is primarily organic-rich, but punctuated by periodic influxes of clastic material marked by peaks in Ti.

Scanning XRF element profiles of Ca and S indicate changes in marine influence (Fig. 8). Extremely high Ca values in Unit I reflect the presence of calcium carbonate as shell material or coatings on mineral grains. Ca ions must have been derived from seawater since there is not a significant terrestrial source. Ca values increase in two steps from the base of Unit I and then rapidly decrease at Unit II when the source of Ca to the sediment is abruptly cut-off. In Unit II and III, Ca values are lower and covary with Ti and PC 1 scores and reflect their minor presence in clastic minerals. PCA performed separately on each Unit (I, II, and III) support these observations (Table 4). The first eigenvector for the PCA of each unit is controlled by a similar suite of elements as observed during the PCA of the entire dataset, but they generally account for a smaller percentage of the total variance (64%, 58%, and 77%, respectively). Ca shows a strong influence on the variance in Units II and III with factor loads greater than 0.950, but in Unit I Ca varies independently showing it is responding to an environmental condition different from the rest of the elements. Sr, also found only in seawater, exhibits similar trends to Ca ($r = 0.96$) since it has the same valence and gets incorporated into calcite.

S can also indicate changes in marine influence since S is primarily a marine-sourced element and should compare with the identification

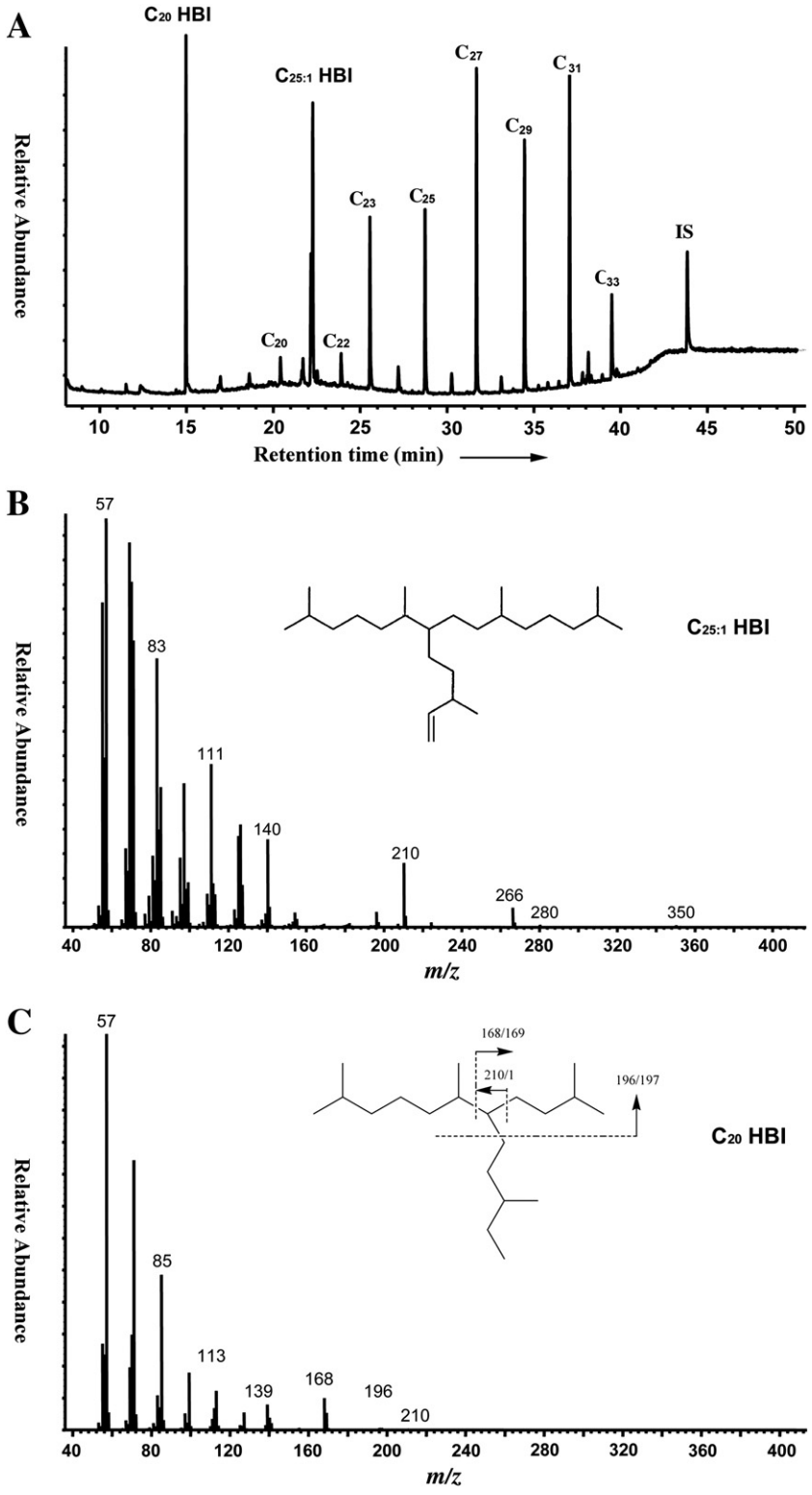

Figure 6. Total ion chromatogram and mass spectra of hydrocarbons in core NHP-207 sediment. (A) Total ion chromatogram showing the presence of *n*-alkanes and highly branched isoprenoids (HBI). (B) Mass spectra show that C_{25} HBIs have a molecular weight 350 ($C_{25}H_{50}$) indicating one unsaturation. A comparison of its mass spectrum with published data (Robson and Rowland, 1986; Xu et al., 2006) suggests that this HBI has a skeleton of 2,6,10,14-tetramethyl-7-(3-methylpentyl) pentadecane and the double bond is most likely located in Δ23–24. (C) The C_{20} HBIs have a unique electron impact spectrum that is characterized by the presence of pairs of ions at *m/z* 168/169, *m/z* 196/197 and *m/z* 210/211. While the molecular ion is undetectable at regular 70 eV ionization, electron ionization at 20 eV and CH_4 chemical ionization revealed a molecular ion of 282, suggesting it is a $C_{20:0}$ alkane and its structure is 2,6,10-trimethyl-7-(3-methylbutyl)-dodecane (Barrick et al., 1980; Yon et al., 1982; Rowland et al., 1985; Rowland and Robson, 1990; Wang and Williams, 2001).

of sulfur during biomarker analysis (Fig. 8). Values are highest in Unit I and sharply decline across Unit II_a. Within Unit II_b values rise to an intermediate level and then decrease at the boundary of Unit III and remain low in the rest of this interval.

The ratio of Si to Ti was plotted to interpret changes in the source of Si in the sediment. Si can be biogenic, primarily from diatoms, or in detrital siliclastic material. Therefore, concentration of Si plotted relative to Ti, which only reflects detrital input, should vary as a

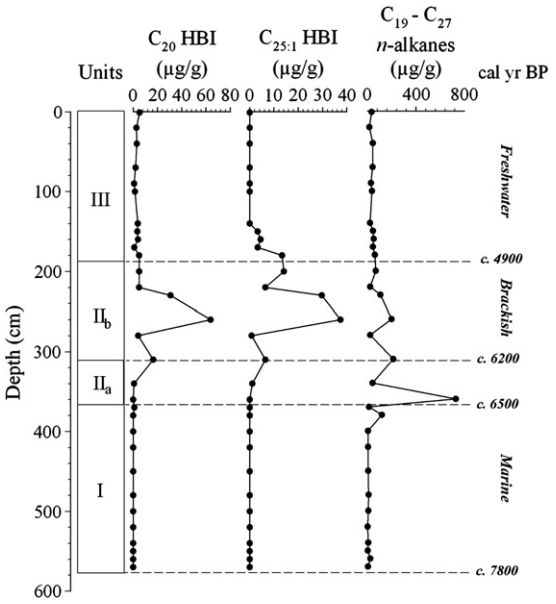

Figure 7. Molecular biomarker concentrations in core NHP-207, including: C_{20} highly branched isoprenoids (HBI), $C_{25:1}$ HBIs, and short and medium-chain *n*-alkanes (C_{19}–C_{27}). C_{20} and $C_{25:1}$ HBIs are typically from marine/brackish diatoms and C_{19}–C_{27} *n*-alkanes are from freshwater algae.

response to changes in the amount of biogenic silica. The relatively low Si/Ti values in Unit I indicate that biogenic silica concentrations were low, but the increase in the ratio across Unit II and the peak in Unit II_b at 270 cm depth indicate that productivity increased and surface water conditions improved for diatoms during this period. The peak in Si/Ti values correlates with changes in the concentration of both HBI biomarkers showing that diatom communities developed rapidly in Unit II. Following this peak in concentration, values gradually decrease across the boundary of Unit III where they stabilize around 140 cm and exhibit only minor fluctuations to the present.

Water column stratification

Water column stratification occurs in isolation basins as dense saline marine water in the monimolimnion becomes trapped beneath a lighter less saline epilimnion as a basin transitions to a restricted marine and then freshwater system. Stratification prevents the complete mixing of the water column and leads to anoxic conditions. Sulfur concentrations and the magnetic susceptibility of the sediment can be used to interpret periods of water column stratification and anoxia. The presence of sulfur in the sediment indicates water column stratification because sulfur reduction only occurs in anoxic environments. In Unit I, elemental sulfur was observed during GC–MS analysis of biomarker samples and high sulfur counts were detected by scanning XRF. This shows that Heimerdalsvatnet was salinity stratified during this interval. Sulfur was not observed in other biomarker samples, but in Unit II, XRF sulfur counts remain elevated compared to the other stratigraphic units. These results could mean that sulfur reduction and stratification also occurred during this period and that lower sulfur values demonstrate a restriction of the source of sulfur.

Magnetic susceptibility can also be used to interpret periods of anoxia. Detrital magnetite, typically the main source of the magnetic signal in sediments, can undergo reductive dissolution in anoxic environments, which is a process that weakens the magnetic susceptibility. Magnetic susceptibility is low in Unit I and lower in Unit II_b. These values contrast those in Units II_a and III and provide further support for the interpretation of water column stratification. However, low magnetic susceptibility can also occur from the dilution of minerogenic input by increased organic sedimentation. Nevertheless, combining results from these two indicators shows that anoxia and reduced mixing occurred within Unit I. The lack of evidence for similar conditions in Units II_a and III shows that the water column was likely not stratified and was fully mixed.

Relative sea-level reconstruction

Our multi-proxy dataset shows that Heimerdalsvatnet was influenced by relative sea-level changes during the Holocene. The three stratigraphic units indicate a regressive sequence from restricted marine to freshwater conditions. Here we use the timing of the transitions between sedimentary units to interpret former sea-level elevations in relation to the threshold of the lake. These are typically referred to as relative sea-level index points, which establish a relationship between a reference tide level and environmental conditions at a site (e.g. Shennan, 1986; Shennan et al., 2000). However, there are uncertainties in the threshold elevation of Heimerdalsvatnet that prohibit strict use of these transitions as sea-level index points. We instead present a more general interpretation of

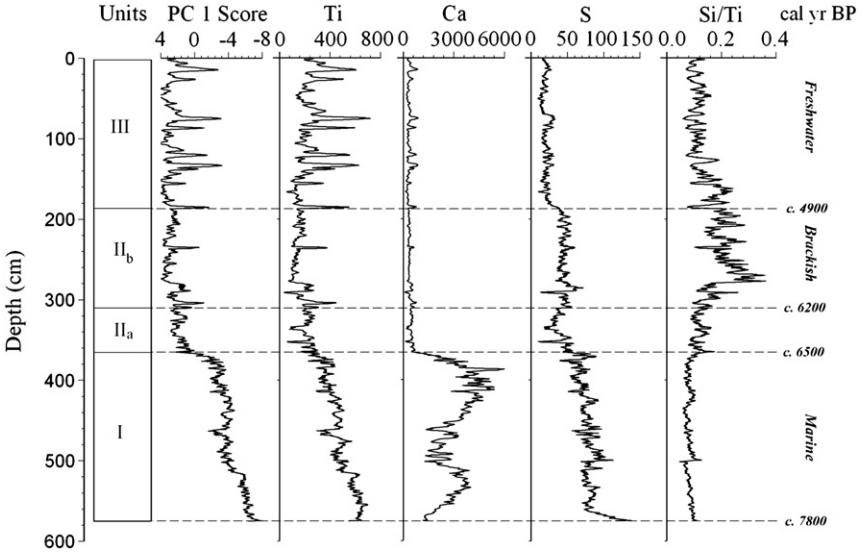

Figure 8. Scanning XRF data from core NHP-207. Scans were conducted at 0.5 mm intervals, but element peak areas are displayed with a 40-sample running average.

Table 3
Correlation coefficients of elements analyzed by scanning XRF. Values with high statistical significant (≥0.90) are in bold.

	Al	Si	S	Cl	K	Ca	Ti	Mn	Fe	Ni	Zn	Br	Rb	Sr
Al	1.00													
Si	−0.15	1.00												
S	−0.49	0.68	1.00											
Cl	−0.29	0.80	0.76	1.00										
K	−0.51	0.80	0.85	0.79	1.00									
Ca	−0.41	0.43	0.74	0.52	0.80	1.00								
Ti	−0.33	0.81	0.70	0.80	**0.93**	0.68	1.00							
Mn	−0.36	0.81	0.77	0.81	**0.93**	0.70	**0.97**	1.00						
Fe	−0.34	0.83	0.81	0.84	**0.92**	0.65	**0.95**	**0.97**	1.00					
Ni	−0.42	0.74	0.78	0.76	**0.93**	0.74	**0.93**	**0.94**	0.94	1.00				
Zn	−0.39	0.80	0.78	0.82	**0.93**	0.68	**0.95**	**0.94**	**0.92**	**0.92**	1.00			
Br	−0.47	0.34	0.81	0.42	0.74	0.89	0.58	0.63	0.61	0.68	0.61	1.00		
Rb	−0.37	0.79	0.63	0.74	**0.90**	0.58	**0.93**	**0.90**	0.87	0.87	0.89	0.47	1.00	
Sr	−0.40	0.54	0.76	0.63	0.87	**0.96**	0.82	0.83	0.78	0.83	0.79	0.86	0.72	1.00

changes in sea-level elevation and compare it to the previously established local sea-level history.

Basin threshold

Heimerdalsvatnet does not have an outlet stream and is a closed basin impounded by a beach ridge (8 m a.s.l.). The lack of an observable bedrock sill complicates the interpretation of former sea-level elevation. We speculate that present lake level (5 m a.s.l.) is controlled by a bedrock sill beneath the beach ridge and is regulated by infiltration through the beach ridge. We acknowledge the uncertainty in the sea-level interpretation from Heimerdalsvatnet, but using an estimate for the threshold elevation (5 m a.s.l.) show that the general sea-level trends correspond with previous reconstructions.

Unit I: Restricted marine phase (7800–6500 cal yr BP)

Diatom assemblages, $\delta^{13}C_{org}$, and Ca and Sr values show that marine influence was greatest from 7800 to 6500 cal yr BP. However, anoxic conditions inferred from low magnetic susceptibility and sulfur data indicate that Heimerdalsvatnet was not a completely open marine system. Restricted marine conditions must have caused salinity stratification of the water column. The presence of a less saline epilimnion is supported by $\delta^{13}C_{org}$ values that are on the low end of Mackie et al.'s (2005) category for marine conditions.

Table 4
Principal component analysis of scanning XRF data from each Unit. Eigenvalues and factor loadings are shown for the 1st principal component. Factor loadings ≥ 0.900 are in bold.

Unit	III	II	I	III–I
Age range (cal yr BP)	0–4900	4900–6500	6500–7800	0–7800
Eigenvalue	9.99	7.51	8.26	9.95
% of variance	76.84	57.78	63.54	76.55
Cumulative %	76.84	57.78	63.54	76.55
Factor Loadings				
Al	0.534	0.067	−0.503	−0.467
Si	0.889	0.364	**0.917**	0.788
S	0.585	0.426	0.692	0.864
K	**0.986**	**0.968**	**0.921**	**0.986**
Ca	**0.983**	**0.956**	−0.414	0.817
Ti	**0.982**	**0.976**	**0.947**	**0.950**
Mn	**0.957**	**0.937**	**0.930**	**0.963**
Fe	**0.928**	0.874	**0.954**	**0.951**
Ni	0.861	0.729	**0.911**	**0.959**
Zn	**0.965**	0.876	0.868	**0.949**
Br	−0.688	0.188	−0.749	0.757
Rb	**0.903**	0.796	0.895	0.889
Sr	**0.965**	0.884	−0.226	**0.900**

Sea level was probably above the threshold of the lake creating a dominantly marine environment, but freshwater input was enough to sustain a density stratified water column. This scenario enables a strong marine sedimentary signal, but shows that direct contact of the monimolimnion with the ocean and oxygenation of the lower water column did not occur during this period. The environment was likely similar to present conditions at outer and inner Borgpollen in Lofoten, a chain of two coastal basins near present sea level (Mills et al., 2009). Inner Borgpollen (Indrepollen) is more isolated and is connected to outer Borgpollen by a small channel. Outer Borgpollen has higher salinity but is also somewhat restricted and is connected to the ocean by two long narrow channels. Outer Borgepollen directly exchanges with the ocean and buffers the marine influence on Indrepollen. However, both are density stratified and anoxic below ~20 m water depth, where sulfur reduction is presently active. Marine influence to outer Borgpollen and Indrepollen varies throughout the year based on tides and the inflow of freshwater. These represent basins that are currently at different stages of isolation and provide an analogue of former conditions at Heimerdalsvatnet.

Unit II: Transitional phase (6500–4900 cal yr BP)

The onset of this phase marks an abrupt decrease in the marine sedimentary signal. Initially, in Unit II_a (6500–6200 cal yr BP) magnetic susceptibility values are higher and there is a dip in S values. Diatoms in this zone are true freshwater species and *n*-alkanes indicate high concentrations of freshwater algae. Although it is difficult to interpret such a brief interval, these conditions might indicate a short period when sea level dropped below the threshold and the lake began to mix or displace the denser monimolimnion.

After 6200 cal yr BP, Unit II_b is characterized by slightly higher C/N ratios, and a rapid rise of Si/Ti, and HBIs. This is accompanied by extremely low magnetic susceptibility and diatoms that have a mix of freshwater and brackish affinities. The apparent rise in biogenic silica, as interpreted from Si/Ti values, is confirmed by the simultaneous increase in the two HBIs. The proliferation of diatoms at this time was likely caused by freshening of the surface water and an increased nutrient supply. An intermittent marine influence from periodic overtopping of the threshold would have delivered saline, nutrient-rich water infrequently to the lake. High productivity in the surface water along with continued meromixis from the re-supply of denser saline water also explains the further reduction of magnetite and/or dilution by high rates of biogenic sedimentation. High productivity and favorable conditions for some diatom species during isolation basin transitions have been recorded elsewhere (e.g. Zong, 1997). In addition, C/N ratios probably reflect instability of the shoreline area around the lake following regression of sea level and prior to soil development, providing another nutrient source.

Unit II_a therefore represents a period when sea level fell below the threshold of the lake and freshwater conditions increased in the epilimnion. Then (Unit II_b) a pause in the rate of emergence and infrequent incursions of seawater, possibly by infiltration through the beach ridge, perpetuated this transitional period. Transitional phases of isolation have also been observed in other locations (e.g. Corner and Haugane, 1993). Commonly, the transition period is brief, but in Heimerdalsvatnet it spanned ~1600 years. Sustained transitional periods observed elsewhere have been interpreted to indicate sea-level stillstands (Corner et al., 1999, 2001; Lloyd, 2000). In Heimerdalsvatnet, our interpretation of a sea-level stillstand is supported by previous investigations (Møller, 1986).

Unit III: Lacustrine phase (4900 cal yr BP – present)

Complete mixing and freshwater conditions began at 4900 cal yr BP. $\delta^{13}C_{org}$ and $\delta^{15}N_{org}$ values reflect freshwater algal sources, diatom floras are entirely freshwater species, and all geochemical properties are more stable during this period. Magnetic susceptibility values show a dramatic increase associated with oxic conditions and periodic detrital input punctuates more organic-rich sedimentation typical of lacustrine environments. Therefore, sea level fell and no longer had any influence on Heimerdalsvatnet. A strong seasonal mixing cycle quickly eroded any remaining water column stratification.

Holocene relative sea level in Lofoten–Vesterålen

Møller (1986) compiled data from the area to create a shoreline displacement curve that summarizes the Holocene relative sea-level history of the Lofoten–Vesterålen archipelago (Fig. 9). The isolation of Heimerdalsvatnet is compared to this curve using a threshold elevation of 5 m a.s.l. and shows that the general trends are similar. Møller's (1986) shoreline displacement curve has a relative sea-level transgression from −3 m in the early Holocene to 9–10 m a.s.l. at ~6800 cal yr BP (Fig. 9). The transgression minimum is constrained by radiocarbon dates on a submarine peat from Petvika in southwestern Vestvågøya (Møller, 1984; Vorren and Moe, 1986) and a peat deposit found buried beneath marine sediment from Ramså on Andøya (Møller, 1986). The transgression maximum is constrained by dates on material found just beneath the highest beach deposits in Ramså (Møller, 1986), from Leknes on Vestvågøya (Møller, 1984), and near Eggum (Bergström, 1973).

Heimerdalsvatnet was a restricted marine environment from 7800 to 6500 cal yr BP. Møller's (1986) shoreline curve shows that relative sea level rose to greater than 5 m around this time and supports the interpretation of marine conditions in Heimerdalsvatnet during Unit I (Fig. 9). We did not recover the transgression contact, but seismic profiles show that our core penetrated the majority of the sedimentary record and %OC and Ca values rise from the base of the core, possibly indicating that inundation of Heimerdalsvatnet occurred shortly before 7800 cal yr BP and corresponding with Møller's (1986) curve. We have no evidence to constrain the upper limit of sea level during the transgression maximum, but assume that maximum wave exposure was at least 8 m a.s.l. corresponding with the elevation of the beach ridge impounding the lake. Following the Tapes maximum at 6800 cal yr BP, there was a sea-level regression of ~4 m (Møller, 1986) (Fig. 9). This is supported by habitation of the Storbåthallaren cave on Flagstadøya dated between 5500 and 5100 cal yr BP (Utne, 1973). Heimerdalsvatnet indicates a regression of sea level, which is marked by the onset of Unit II at 6500 cal yr BP, when the basin experienced greater freshwater conditions and only periodic marine influence, but it occurred more rapidly than expressed by the Møller (1986) sea-level curve. The dates from Storbåthallaren cave were used to suggest sea level was near or below ~7.6 m during the period it was inhabited, ~400 years. This period defines a sea-level stillstand in Møller's (1986) shoreline curve and closely corresponds with the duration of Unit II in Heimerdalsvatnet, from 6500 to 4900 cal yr BP. There is also evidence for a short transgressive phase at, ~5100 cal yr BP (Marthinussen, 1962; Møller, 1984), but there is no indication of a change in conditions at Heimerdalsvatnet. Following this stillstand, sea level regressed through the late Holocene (Marthinussen, 1962), which corresponds to the complete isolation of Heimerdalsvatnet at 4900 cal yr BP. Differences between these sea-level curves are a result of uncertainties in the threshold elevation of Heimerdalsvatnet and how representative the Møller (1986) curve is for this exact area.

Conclusions

The isolation sequence of Heimerdalsvatnet was analyzed using a variety of analytical techniques. Physical, organic geochemical, and diatom analyses defined three litho/chemo-stratigraphic units related

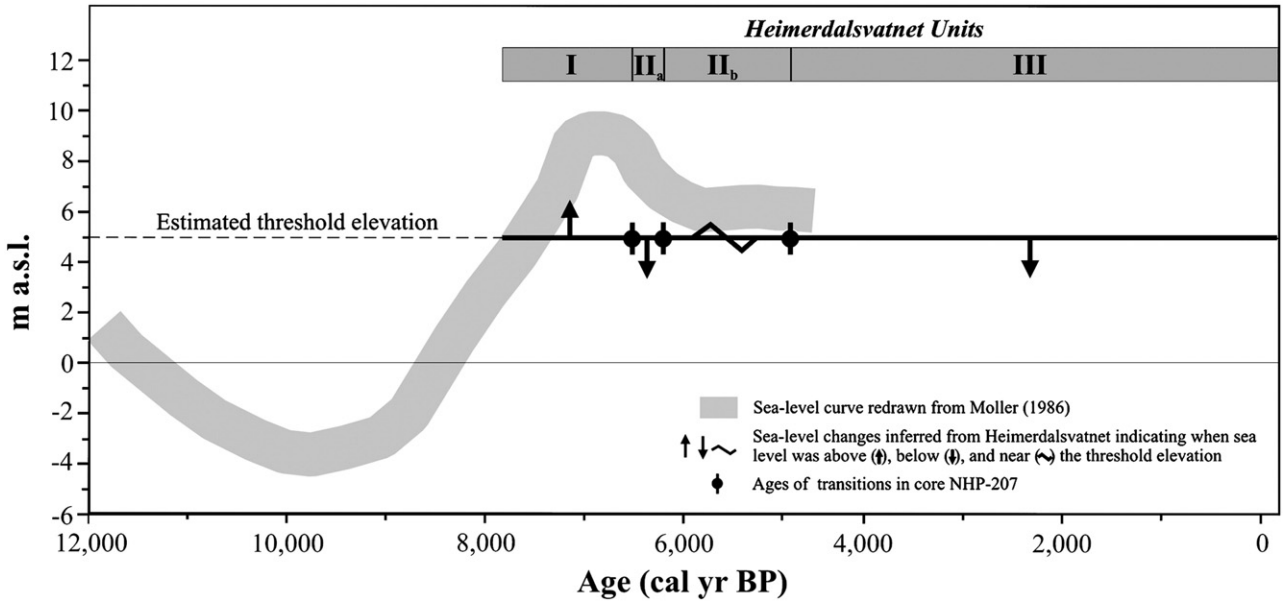

Figure 9. Generalized shoreline displacement curve redrawn from Møller (1986) and converted to calendar years and the record of sea-level change interpreted from Heimerdalsvatnet assuming a threshold elevation of 5 m a.s.l.

to sea-level lowering following the Tapes transgression. This multi-proxy approach provides a detailed view of paleoenvironmental conditions and allows us to compare methods of assessing isolation basin stratigraphy directly.

Diatoms are reliable indicators of salinity and select samples provided an overall understanding of salinity changes across the record and supported the interpretation of other proxies. Bulk organic geochemical data, mainly $\delta^{13}C$, exhibited expected trends from marine to freshwater environments and showed clear changes at stratigraphic boundaries further validating these techniques in isolation basin studies. Molecular biomarkers produced by brackish and freshwater algae were also analyzed and are a new approach to characterizing isolation basin stratigraphy. Concentrations of HBIs and *n*-alkanes varied dramatically across the record and indicated changes in surface water conditions during isolation. There is great potential for the use of these and other molecular biomarkers in isolation basin studies. Although, the extraction, analysis, and identification of organic molecules is labor intensive, biomarker proxies can add a new understanding of paleoenvironmental conditions or be applied where there are uncertainties in microfossil or bulk organic geochemical data. Scanning XRF is a rapid, high-resolution technique for defining changes in sediment composition. We presented a statistical approach using elemental data to classify stratigraphic units and to characterize the response of different elements. The elemental dataset had a strong detrital signal, but profiles of Ca and Sr showed significantly different trends related to changes in marine influence and Si/Ti seemed to indicate changes in biogenic silica.

Results from our analysis demonstrate that Heimerdalsvatnet was a restricted marine basin from 7800 to 6500 cal yr BP. Evidence for anoxia during this period indicates that conditions resembled the present-day environments in two nearby coastal basins. Following the transgression sea level lowered, but marine water still had periodic influence on Heimerdalsvatnet from 6500 to 4900 cal yr BP before it was fully isolated at 4900 cal yr BP. Despite uncertainties in the threshold elevation, these intervals correspond with general trends in the local sea-level history.

Acknowledgments

This project was funded by National Science Foundation Grants ARC-0714014 and ARC-0454959, National Oceanic and Atmospheric Administration grant NA06OAR4310173, a GSA Graduate Student Research Grant, a GSA Quaternary Geology and Geomorphology Division J. Hoover Mackin Research Award, a Sigma-Xi Grant-in-Aid of Research, a UMass Department of Geosciences Leo M. Hall Memorial Grant, and was completed while NLB was supported by a U.S. Fulbright Program fellowship. We thank Jon Pilcher for his help interpreting tephra data, Arnt Solheim for providing access to Heimerdalsvatnet, Geir Are Johansen and Lars Erik Narmo of the Lofotr Viking Museum for logistical support, Pierre Metzger for running GC–MS chemical ionization, Tim Cook and Sarah Balascio for assistance in the field, and Jerry Lloyd and one anonymous reviewer for helpful comments on an earlier draft.

References

Alloway, B.V., Larsen, G., Lowe, D.J., Shane, P.A.R., Westgate, J.A., 2006. Tephrochronology. In: Elias, S.A. (Ed.), Encyclopedia of Quaternary Science. Elsevier, Oxford, pp. 2869–2898.

Bargel, T.H., 2003. Quaternary geological mapping of Fennoscandia and Nordland: deglaciation, deposits, stratigraphy and applications. Ph.D. thesis. Department of Geology and Mineral Resources Engineering, Norwegian University of Science and Technology, pp. 324.

Barrick, R.C., Hedges, J.I., Peterson, M.L., 1980. Hydrocarbon geochemistry of the Puget Sound region. 1. Sedimentary acyclic hydrocarbons. Geochim. Cosmochim. Acta 44, 1349–1362.

Bendle, J.A.P., Rosell-Melé, A., Cox, N.J., Shennan, I., 2009. Alkenones, alkenoates and organic matter in coastal environments of N.W. Scotland: assessment of potential application for sea-level reconstruction. Geochem. Geophys. Geosyst. 10, Q12003.

Bergström, E., 1973. Den prerecenta lokalglaciationens utbredningshistoria inom Skanderna. Naturgeografiska institutionen, University of Stockholm. Forskningsrapport 16, 214.

Corner, G.D., Haugane, E., 1993. Marine-lacustrine stratigraphy of raised coastal basins and postglacial sea-level change at Lyngen and Vanna, Troms, northern Norway. Nor. Geol. Tidsskr. 73, 175–197.

Corner, G.D., Yevzerov, V.Y., Kolka, V.V., Møller, J.J., 1999. Isolation basin stratigraphy and Holocene relative sea-level change at the Norwegian-Russian border north of Nikel, northwest Russia. Boreas 28, 146–166.

Corner, G.D., Kolka, V.V., Yevzerov, V.Y., Møller, J.J., 2001. Postglacial relative sea-level change and stratigraphy of raised coastal basins on Kola Peninsula, northwest Russia. Glob. Planet. Change 31, 155–177.

Croudace, I.W., Rindby, A., Rothwell, R.G., 2006. ITRAX: description and evaluation of a new multi-function X-ray core scanner. In: Rothwell, R.G. (Ed.), New Techniques in Sediment Core Analysis. Geological Society, London, Special Publications, 267, pp. 51–564.

Davies, S.M., Elmquist, M., Bergman, J., Wohlfarth, B., Hammarlund, D., 2007. Cryptotephra sedimentation processes within two lacustrine sequences from west central Sweden. Holocene 17, 319–330.

Gearing, P.J., Gearing, J.N., Lytle, T.F., Lytle, J.S., 1976. Hydrocarbons in 60 north east Gulf of Mexico Shelf sediments: a preliminary study. Geochimica et Cosmochim Acta 40, 1005–1017.

Hall, V.A., Pilcher, J.R., 2002. Late-Quaternary Icelandic tephras in Ireland and Great Britain: detection, characterization and usefulness. Holocene 12, 223–230.

Hutchinson, I., James, T.S., Clague, J.J., Barrie, J.V., Conway, K.W., 2004. Reconstruction of late Quaternary sea-level change in southwestern British Columbia from sediments in isolation basins. Boreas 33, 183–194.

Kjemperud, A., 1981. Diatom changes in sediments of basins possessing marine/lacustrine transitions in Frosta, Nord-Troendelag, Norway. Boreas 10, 27–38.

Lamb, A.L., Wilson, G.P., Leng, M.J., 2006. A review of coastal paleoclimate and relative sea-level reconstructions using $\delta^{13}C$ and C/N ratios in organic material. Earth Sci. Rev. 75, 29–57.

Larsen, G., Newton, A.J., Dugmore, A.J., Vilmundardóttir, E.G., 2001. Geochemistry, dispersal, volumes and chronology of Holocene silicic tephra layers from the Katla volcanic system, Iceland. J. Quatern. Sci. 16, 119–132.

Lloyd, J., 2000. Combined foraminiferal and thecamoebian environmental reconstruction from an isolation basin in NW Scotland: implications for sea-level studies. J. Foramin. Res. 30, 294–305.

Long, A.J., Roberts, D.H., Wright, M.R., 1999. Isolation basin stratigraphy and Holocene relative sea-level change on Arveprinsen Ejland, Disko Bugt, West Greenland. J. Quatern. Sci. 14, 323–345.

Mackie, E.A.V., Leng, M.J., Lloyd, J.M., Arrowsmith, C., 2005. Bulk organic $\delta^{13}C$ and C/N ratios as palaeosalinity indicators within a Scottish isolation basin. J. Quatern. Sci. 20, 303–312.

Mackie, E.A.V., Lloyd, J.M., Leng, M.J., Bentley, M.J., Arrowsmith, C., 2007. Assessment of $\delta^{13}C$ and C/N ratios in bulk organic matter as palaeosalinity indicators in Holocene and Lateglacial isolation basin sediments, northwest Scotland. J. Quatern. Sci. 22, 579–591.

Marthinussen, M., 1962. 14C-datings referring to shore lines, transgressions and glacial substages in northern Norway. Nor. Geol. Unders. 215, 37–67.

Meyers, P.A., 1994. Preservation of elemental and isotopic source identification of sedimentary organic matter. Chem. Geol. 114, 289–302.

Meyers, P.A., 2003. Applications of organic geochemistry to paleolimnological reconstructions: a summary of examples from the Laurentian Great Lakes. Org. Geochem. 34, 261–289.

Mills, K., Mackay, A.W., Bradley, R.S., Finney, B., 2009. Diatom and stable isotope records of late-Holocene lake ontogeny at Indrepollen, Lofoten, NW Norway: a response to glacio-isostasy and Neoglacial cooling. Holocene 19, 261–271.

Møller, J.J., 1984. Holocene shore displacement at Nappstraumen, Lofoten, North Norway. Nor. Geol. Tidsskr. 64, 1–5.

Møller, J.J., 1985. Coastal caves and their relation to early postglacial shore levels in Lofoten and Vesterålen, North Norway. Nor. Geol. Unders. 400, 51–65.

Møller, J.J., 1986. Holocene transgression maximum about 6000 years BP at Ramså, Vesterålen, North Norway. Nor. Geogr. Tidsskr. 40, 77–84.

Møller, J.J., 1987. Shoreline relation and prehistoric settlement in northern Norway. Nor. Geogr. Tidsskr. 41, 45–60.

Møller, J.J., 1989. Geometric simulation and mapping of Holocene relative sea-level changes in northern Norway. J. Coast. Res. 5, 403–417.

Pilcher, J.R., Hall, V.A., McCormac, F.G., 1996. An outline tephrochronology for the Holocene of the north of Ireland. J. Quatern. Sci. 11, 485–494.

Pilcher, J., Bradley, R.S., Francus, P., Anderson, L., 2005. A Holocene tephra record from the Lofoten Islands, Arctic Norway. Boreas 34, 136–156.

Plunkett, G.M., Pilcher, J.R., McCormac, F.G., Hall, V.A., 2004. New dates for the first millennium BC tephra isochrones in Ireland. Holocene 14, 780–786.

Reimer, P.J., Baillie, M.G.L., Bard, E., Bayliss, A., Beck, J.W., Bertrand, C.J.H., Blackwell, P.G., Buck, C.E., Burr, G.S., Cutler, K.B., Damon, P.E., Edwards, R.L., Fairbanks, R.G., Friedrich, M., Guilderson, T.P., Hogg, A.G., Hughen, K.A., Kromer, B., McCormac, F.G., Manning, S.W., Ramsey, C.B., Reimer, R.W., Remmele, S., Southon, J.R., Stuiver, M., Talamo, S., Taylor, F.W., van der Plicht, J., Weyhenmeyer, C.E., 2004. IntCal04 Terrestrial radiocarbon age calibration, 26–0 ka BP. Radiocarbon 46, 1029–1058.

Renberg, I., 1990. A procedure for preparing large sets of diatom slides from sediment cores. J. Paleolimnol. 4, 87–90.

Robson, J.N., Rowland, S.J., 1986. Identification of novel widely distributed sedimentary acyclic sesterterpenoids. Nature 324, 561–563.

Rowland, S.J., Robson, J.N., 1990. The widespread occurrence of highly branched acyclic C_{20}, C_{25} and C_{30} hydrocarbons in recent sediments and biota-a review. Mar. Environ. Res. 30, 191–216.

Rowland, S.J., Yon, D.A., Lewis, C.A., Maxwell, J.R., 1985. Occurrence of 2, 6, 10-trimethyl-7-(3-methylbutyl)-dodecane and related hydrocarbons in the green alga Enteromorpha prolifera and sediments. Org. Geochem. 8, 207–213.

Shennan, I., 1986. Flandrian sea-level changes in the Fenland. II: Tendencies of sea-level movement, altitudinal changes, and local and regional factors. J. Quatern. Sci. 1, 155–179.
Shennan, I., Innes, J.B., Long, A.J., Zong, Y., 1995. Holocene relative sea-level changes and coastal vegetation history at Kentra Moss, Argyll, northwest Scotland. Marine Geology 124, 43–59.
Shennan, I., Horton, B., Innes, J., Gehrels, R., Lloyd, L., McArthur, J., Rutherford, M., 2000. Late Quaternary sea-level changes, crustal movements and coastal evolution in Northumberland, UK. J. Quatern. Sci. 15, 215–237.
Sparrenbom, C.J., Bennike, O., Björk, S., Lambeck, K., 2006. Holocene relative sea-level changes in the Qaqortoq area, southern Greenland. Boreas 35, 171–187.
Stuiver, M., Reimer, P.J., 1993. Extended 14C database and revised CALIB radiocarbon calibration program. Radiocarbon 35, 215–230.
Svendsen, J.I., Mangerud, J., 1990. Sea-level changes and pollen stratigraphy on the outer coast of Sunnmøre, western Norway. Nor. Geol. Tidsskr. 70, 111–134.
Talbot, M.R., 2001. Nitrogen isotopes in palaeolimnology. In: Last, W.M., Smol, J.P. (Eds.), Tracking Environmental Change Using Lake Sediments. Volumne 2: Physical and Geochemical Methods. Kluwer Academic Publishers, Dordrecht, The Netherlands, pp. 401–439.
Turney, C.S.M., 1998. Extraction of rhyolitic component of Vedde microtephra from minerogenic lake sediments. J. Paleolimnol. 19, 199–206.
Utne, A., 1973. En veidekulturs-boplass I Lofoten. University of Tromsø, Storbåthallaren ved Nappstraumen. Thesis.
Vestøl, O., 2006. Determination of postglacial land uplift in Fennoscandia from leveling, tide-gauges and continuous GPS stations using least squares collocation. J. Geodesy 80, 248–258.
Vorren, K.-D., Moe, D., 1986. The early Holocene climate and sea-level changes in Lofoten and Vesterålen, North Norway. Nor. Geol. Tidsskr. 66, 135–143.
Vorren, T.O., Vorren, K.-D., Alm, T., Gulliksen, S., Løvlie, R., 1988. The last deglaciation (20, 000 to 11, 000 B.P.) on Andøya, northern Norway. Boreas 17, 41–77.
Wang, R.L., Williams, W.D., 2001. Biogeochemical changes in the sediments of Lake Cantara South, a saline lake in South Australia. Hydrobiologia 457, 17–24.
Westman, P., Hedenström, A., 2002. Environmental changes during isolation processes from the Litorina Sea as reflected by diatoms and geochemical parameters — a case study. Holocene 12, 531–540.
Wilson, G.P., Lamb, A.L., Leng, M.J., Gonzalez, S., Huddart, D., 2005. $\delta^{13}C$ and C/N as potential coastal palaeoenvironmental indicators in the Mersey Estuary, UK. Quatern. Sci. Rev. 24, 2015–2029.
Xu, Y.P., Jaffe, R., Wachnicka, A., Gaiser, E.E., 2006. Occurrence of C_{25} highly branched isoprenoids (HBIs) in Florida Bay: paleoenvironmental indicators of diatom-derived organic matter inputs. Org. Geochem. 37, 847–859.
Yon, D.A., Maxwell, J.R., Ryback, G., 1982. 2, 6, 10-trimethyl-7-(3-methylbutyl)-dodecane, a novel sedimentary biological marker compound. Tetrahedron Lett. 23, 2143–2146.
Zhang, Z., Sachs, J.P., 2007. Hydrogen isotope fractionation in freshwater algae: I. Variations among lipids and species. Org. Geochem. 38, 582–608.
Zhang, Z.H., Zhao, M.X., Yang, X.D., Wang, S.M., Jiang, X.H., Oldfield, F., Eglinton, G., 2004. A hydrocarbon biomarker record for the last 40 kyr of plant input to Lake Heqing, southwestern China. Org. Geochem. 35, 595–613.
Zong, Y., 1997. Implications of *Paralia Sulcata* abundance in Scottish isolation basin studies. Diatom Res. 12, 125–150.
Zong, Y., Horton, B.P., 1999. Diatom-based tidal-level transfer functions as an aid in reconstructing Quaternary history of sea-level movements in the UK. J. Quatern. Sci. 14, 153–167.